Elasticity of smectic-*A* elastomers

J. M. Adams and M. Warner
Cavendish Laboratory, University of Cambridge, Madingley Road, Cambridge CB3 0HE, United Kingdom
(Received 3 November 2004; published 23 February 2005)

We present a fully nonlinear model of the elasticity smectic-*A* elastomers, and compare our results with a wide range of experimental observations: extreme Poisson ratios, the in-plane modulus, the modulus before and after threshold to layer rotation in response to stretches along the layer normal, the threshold strain, the characteristic, and singular rotation of layers after the threshold. We calculate the x-ray scattering from rotating layers and compare with available data. The model is derived in two ways: from geometrical constraints imposed by layers on a nematic elastomer, and from application of statistical mechanics to a microscopic model of the effect of crosslink points confined in a corrugated potential.

DOI: 10.1103/PhysRevE.71.021708 PACS number(s): 61.30.Cz, 61.41.+e, 61.10.Eq, 81.40.Jj

I. INTRODUCTION

Elastomers are crosslinked networks of polymer chains. They are capable of huge distortions, hence their elasticity is nonlinear for both geometrical and material reasons. They are soft solids in the sense that their shear moduli are much less than the bulk moduli whereupon they deform at essentially constant volume. This third source of nonlinearity makes still further inadequate any linear continuum picture of most rubber elastic phenomena.

We present a fully nonlinear, statistical mechanical theory of elasticity of particularly complex elastomers–smectic-*A* (Sm-*A*) rubbers. Such elastomers have 1D layering order superimposed upon the nematic rubber elasticity of the underlying matrix. Thus, the material is itself complex in that it is both rubbery (with the capacity for elastic nonlinearity mentioned above) and has an internal degree of freedom, its nematic ordering director. Its nematic order is independently mobile but also coupled to the solid matrix. This is possible since a rubber is liquid-like at the local molecular level though it cannot flow in any macroscopic sense. The director can be induced to rotate by imposed strains. Indeed its motion can cause some special shape changes to occur at zero energy cost. These have been observed over huge ranges of strain and have a characteristic, universal strain-angle dependence. We shall see strain-induced director motion but not soft elasticity—the added constraint of the layers which are coupled to the solid matrix and to the director make soft trajectories impossible in Sm-*A*. A later paper will deal with Sm-*C* elastomers which can deform softly because of their lower point symmetry.

Experiment can give clear guidance for theory in the limit of strong coupling between smectic order and the rubbery matrix. Stretching along the layer normal [see Fig. 1(a)] of an elastomer with strong smectic effects [1] initially has a higher associated modulus, comparable to the smectic layer modulus $B \sim 10^7$–10^8 Pa observed in liquid Sm-*A*. This is significantly less than the bulk modulus of rubber and hence distortions still have constant volume. Thus the Poisson ratios are initially $(1/2,1/2)$ associated with volume-conserving contractions in the essentially fluid (rubbery) smectic planes. On the other hand, B is almost 10^2 times larger than underlying rubber's shear moduli which themselves scale with the single (shear) modulus $\mu \sim 10^5$–10^6 Pa characterizing any isotropic state of the elastomer. At relatively small strain on a rubbery scale ($\sim 5\%$) there is an instability which causes the layers to start rotating in order to relieve the stiff layer dilation deformation in favor of lower cost rubber distortions at constant layer spacing. This response is the rubbery equivalent of the classical instability to avoid layer dilation predicted and observed in liquid smectics by Clark and Meyer [2] and which has analogy to the Helfrich-Hurault instability found in liquid cholesterics. We shall call this the CMHH instability and return to it at some length in Sec. III A, Sec. III E 1 (where we give a geometrical explanation) and in Sec. IV D. Section IV makes contact with experiment; we analyze the elastic response and the x-ray data [1] but, unlike these authors, conclude that the layers rotate rather than melt. This is consistent with the fact that smectic ordering is of the order of 10^2 times more rigid than the rubbery scale. The rotation is seen both in x rays and optically. When the smectic modulus is large, one can think of smectic elastomers as being two-dimensional but where the orientation of these two dimensions can be mobile.

Although chains are highly mobile (Sm-*A* elastomers can suffer huge reversible deformations), the above evidence shows that crosslinks, which create and define the rubbery solid, are strongly pinned by smectic layers. It is not possible to stretch along the layer normal and have the crosslinks glide through layers. The associated modulus is therefore not rubbery; it is rather that of the smectic layers. In Sec. V we calculate from a molecular model the consequences of this pinning: (i) the coupling between layer and matrix displacements characterized by the modulus Λ, first introduced in [3], which we estimate; (ii) the strict geometrical constraints when deformations are imposed crosslinks must respect the layer positions and hence the matrix must sense layer spacings; (iii) the layer normal and the director are rigidly identified with each other.

The second example of a constrained response is stretching in one direction in the plane, see Fig. 1(b). Contraction is only in the perpendicular direction in the plane and not at all along the layer normal. Hence for small deformations where the Poisson ratios are defined, they take the extreme values

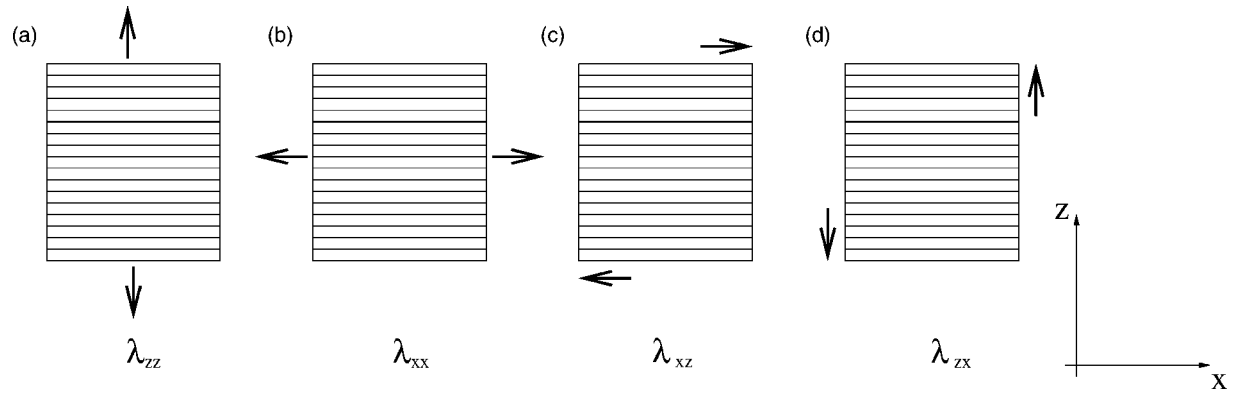

FIG. 1. Imposed deformation; (a) stretching parallel to the layer normal; (b) stretching perpendicular to the layer normal; (c) shearing the layers in their plane; and (d) shear out of the planes.

(1, 0) as is known from the remarkable experiments of the Finkelmann group [1,4]. Analogous response continues into the nonlinear regime and the associated modulus is rubbery. Whether deformations are large or small, we essentially have a 2D rubber when smectic-matrix coupling is strong.

The third and fourth deformations we shall consider are imposed shears λ_{xz} and λ_{zx}, Figs. 1(c) and 1(d), where z is the layer normal and x a direction in the smectic planes. These two shears have very different effects on the layer orientation and spacing. We conclude Sec. III with a general decomposition of deformations into components that are differentiated in their effect on the layer normal.

II. LARGE STRAIN MODEL OF SMECTIC-*A* ELASTOMERS

Linear continuum models, using symmetrized strain tensors, for smectic elastomers were developed many years ago [3,5–7]. They can offer guidance, for instance through the use of group-theoretical analysis of terms permitted in their invariant free energy. However, such theories suffer the essential limitations of linearity mentioned above. Nonlinear elasticity using nonlinear symmetrized strain tensors can be also be developed [8]. One then expands the free energy phenomenologically, say to quartic order. This is sufficient for many purposes, for instance to govern instabilities that arise at quadratic order.

We shall retain Cauchy deformation gradient tensors $\underline{\underline{\lambda}}$ that directly show the shape change of the body and retain information (because they are not symmetrized) of any rotations of the reference space. It is convenient to record shape changes of a reference space considered *after* any phase transitions (with, e.g., spontaneous elongation) might have taken place. These are the as-imposed shape changes. (There are, however, deep theoretical reasons that are the basis of soft elasticity [8,9] for taking deformations with respect to the body before symmetry breaking, see also [10] for an overview.) Recording rotations is also useful since they can be with respect to internal degrees of freedom, for instance the director. Such relative rotations enter the nematic rubber elastic free energy, see for instance a continuum example [11] and are also central to nematic elastomers at large deformations [10]. We retain the essential ideas of nematic rubber elasticity but take account also of the rigid constraints added in by coupling to the smectic layers. We thus follow the strategy of earlier continuum approaches, in particular that of [7] which gives molecular estimates of linear moduli and also discusses relative rotations in the smectic context. Here however we suppress the freedom of layers and the nematic director to relatively rotate. Our rigidly coupled smectic layers have the director rigidly identified with the layer normal ($b_\perp \to \infty$ in the notation of [7]). Thus, there will be no partial renormalization of the shear modulus that would otherwise lead to soft elasticity in a nematic system ([7] discusses the smectic effects on this renormalization).

We defer (to Sec. V) a molecular model that shows how chains strongly coupled to the layer system generate the rigid constraints we study in this section.

A. Layer constraints and smectic energy

If layers are rigidly embedded in the network, then deformations $\underline{\underline{\lambda}}$ will induce layer spacing changes, which we now calculate in a frame independent form, in order to find the associated smectic energy (proportional to the layer modulus B). Any material point in the layer deforms as $\mathbf{x} \to \underline{\underline{\lambda}} \cdot \mathbf{x}$. Any two perpendicular unit vectors in the plane of the smectic layer, $\mathbf{k}$ and $\mathbf{m}$ say, define the layer normal $\mathbf{n}_0 = \mathbf{k} \times \mathbf{m}$. Since the vectors deform with the plane, the cross product of the deformed vectors defines the new normal, $\mathbf{n}$,

$$\mathbf{n} = \frac{(\underline{\underline{\lambda}} \cdot \mathbf{k}) \times (\underline{\underline{\lambda}} \cdot \mathbf{m})}{|(\underline{\underline{\lambda}} \cdot \mathbf{k}) \times (\underline{\underline{\lambda}} \cdot \mathbf{m})|} \tag{1}$$

as illustrated in Fig. 2.

Writing $\mathrm{Det}(\underline{\underline{\lambda}})\epsilon_{ijk} = \epsilon_{\alpha\beta\gamma}\lambda_{\alpha i}\lambda_{\beta j}\lambda_{\gamma k}$, using $\mathrm{Det}(\underline{\underline{\lambda}}) = 1$, and multiplying from the right by $(\underline{\underline{\lambda}}^{-1})_{kp}$ yields

$$\epsilon_{\alpha\beta p}\lambda_{\alpha i}\lambda_{\beta j} = \lambda_{kp}^{-1}\epsilon_{ijk} = \lambda_{pk}^{-T}\epsilon_{ijk}. \tag{2}$$

We denote by $\underline{\underline{\lambda}}^{-T}$ the transpose of the inverse of $\underline{\underline{\lambda}}$ [i.e., the cofactor tensor, since $\mathrm{Det}(\underline{\underline{\lambda}}) = 1$]. Substituting Eq. (2) into the cross products in $\mathbf{n}$ above and setting $\mathbf{k} \times \mathbf{m} = \mathbf{n}_0$ gives

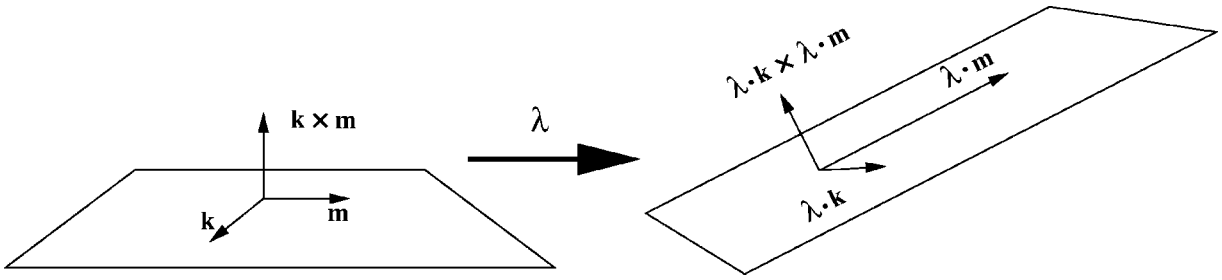

FIG. 2. The normal to the layer deforms when the vectors in the layer deform according to $\mathbf{x} \rightarrow \underline{\underline{\lambda}} \cdot \mathbf{x}$.

$$\mathbf{n} = \frac{\underline{\underline{\lambda}}^{-T} \cdot \mathbf{n}_0}{|\underline{\underline{\lambda}}^{-T} \cdot \mathbf{n}_0|}. \tag{3}$$

Layer normals thus deform according to $\underline{\underline{\lambda}}^{-T}$.

We can calculate the spacing between two planes in the deformed smectic elastomer. Consider the material points $\mathbf{x}$ and $\mathbf{x}+d_0\mathbf{n}_0$ in two adjacent planes. These transform into $\underline{\underline{\lambda}} \cdot \mathbf{x}$ and $\underline{\underline{\lambda}} \cdot \mathbf{x} + d_0 \underline{\underline{\lambda}} \cdot \mathbf{n}_0$, respectively. Resolving along the new layer normal the difference between these two deformed points gives the new layer spacing

$$d = d_0(\underline{\underline{\lambda}} \cdot \mathbf{n}_0) \cdot \mathbf{n} = d_0(\underline{\underline{\lambda}} \cdot \mathbf{n}_0) \cdot \frac{\underline{\underline{\lambda}}^{-T} \cdot \mathbf{n}_0}{|\underline{\underline{\lambda}}^{-T} \cdot \mathbf{n}_0|},$$

$$d/d_0 = \frac{1}{|\underline{\underline{\lambda}}^{-T} \cdot \mathbf{n}_0|}. \tag{4}$$

Concrete examples are easy to evaluate since $|\underline{\underline{\lambda}}^{-T} \cdot \mathbf{n}_0|$ arose from the normalization $|(\underline{\underline{\lambda}} \cdot \mathbf{k}) \times (\underline{\underline{\lambda}} \cdot \mathbf{m})|$ in Eq. (1). Taking $\mathbf{k}=\mathbf{x}$ and $\mathbf{m}=\mathbf{y}$, and hence $\mathbf{n}_0=\mathbf{z}$, then

$$\frac{d}{d_0} = \frac{1}{|\epsilon_{ijk}\lambda_{jx}\lambda_{ky}|}, \quad n_i = \frac{\lambda_{iz}^{-T}}{|\epsilon_{ijk}\lambda_{jx}\lambda_{ky}|}, \tag{5}$$

expressions we shall repeatedly use. The cross product expression that produces the new layer normal can be thought of geometrically as calculating the distance along the normal between two planes, or as calculating the area of the plane which relates to the physical constraint of constant volume.

B. Rubber elastic free energy

Smectic rubbers are capable of large, reversible shape changes, presumably because their chains are still Gaussian and highly mobile. Additionally the smectic has the spontaneous uniaxial orientational order of a nematic. Hence we expect, approximately, to have a nematic elastomer for the underlying matrix, with the stringent constraints of layers explored above. Describing shape change by $\underline{\underline{\lambda}}$, an appropriate free energy density is given by the trace formula [10]

$$f_n = \frac{1}{2}\mu \, \mathrm{Tr}(\underline{\underline{\lambda}} \cdot \underline{\underline{l}}_0 \cdot \underline{\underline{\lambda}}^T \cdot \underline{\underline{l}}^{-1}), \tag{6}$$

where $\underline{\underline{l}}_0$ is the shape tensor describing the distribution of chain conformations before deformation; $\underline{\underline{l}}$ describes that afterward

$$\underline{\underline{l}}_0 = (r-1)\mathbf{n}_0\mathbf{n}^T + \underline{\underline{\delta}}, \tag{7}$$

$$\underline{\underline{l}} = (r-1)\mathbf{n}\,\mathbf{n}^T + \underline{\underline{\delta}}. \tag{8}$$

The order is characterized by an ordering direction $\mathbf{n}_0$ (which becomes $\mathbf{n}$) and a shape anisotropy of the chain shape distribution

$$r = \ell_\parallel/\ell_\perp = \langle R_\parallel^2 \rangle / \langle R_\perp^2 \rangle. \tag{9}$$

This single parameter is the ratio of the effective step lengths parallel ($\ell_\parallel$) and perpendicular ($\ell_\perp$) to the director, themselves related to the mean square chain dimensions in these directions. One can measure r by neutron scattering directly, or deduce it from thermal expansion measurements on going from the isotropic to nematic/smectic states. Values of r have been observed between 1.05–60 according to chain type in the prolate case; oblate chains have $r<1$. Smectic elastomer thermal expansions [1] suggest prolate chains with $r \sim 2$, an illustrative value we shall adopt in this paper. The trace formula describes a wide range of complex, nonlinear phenomena in nematic elastomers including large thermal expansions, singular director rotations and plateaux in stress-strain relations over wide ranges and geometries of strain. We shall assume that applied strains do not change the magnitude of the nematic order, at most affecting its direction. This is a good assumption if we are far from the nematic-isotropic transition. The free energy (6) is rederived in Sec. V in the process of describing the smectic constraints.

III. RESPONSE OF A SMECTIC *A* ELASTOMER TO IMPOSED STRAIN

We impose one component of $\underline{\underline{\lambda}}$ (identified as a λ without suffixes) as in Fig. 1 and calculate the relaxation of the other components—that is shape changes and rotation of the layers and hence also of the solid. One also obtains the stress required to impose λ. The free energy density (with the reduced layer compression modulus $b=B/\mu$)

$$f = \frac{1}{2}\mu[\mathrm{Tr}(\underline{\underline{\lambda}} \cdot \underline{\underline{l}}_0 \cdot \underline{\underline{\lambda}}^T \cdot \underline{\underline{l}}^{-1}) + b(d/d_0 - 1)^2] \tag{10}$$

is minimized subject to volume conservation $\mathrm{Det}[\underline{\underline{\lambda}}]=1$ and where the relative layer spacing change and the new director are given by Eqs. (3) and (4). The last two conditions arise from the affine deformation of the layer system with the strain, which we prove in Sec. V. The reduced layer modulus can be large but presumably vanishes as one approaches the Sm-*A*–nematic transition where also the affine layer deformation assumption would become invalid.

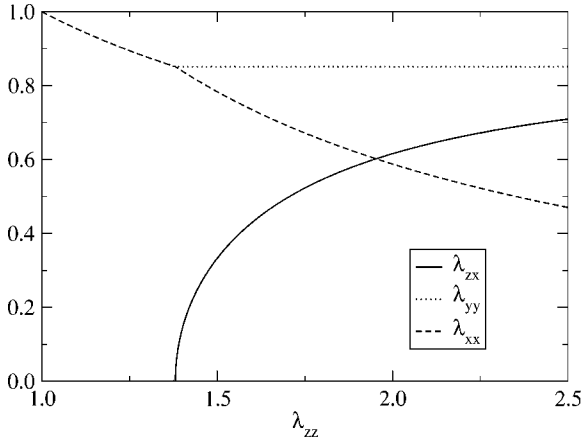

FIG. 3. Deformation tensor components for an imposed λ_{zz} for $b=5$ and $r=2$. The shear λ_{zx} relaxes to an asymptote of $1/\sqrt{\lambda_{cr}}$ for large λ_{zz}.

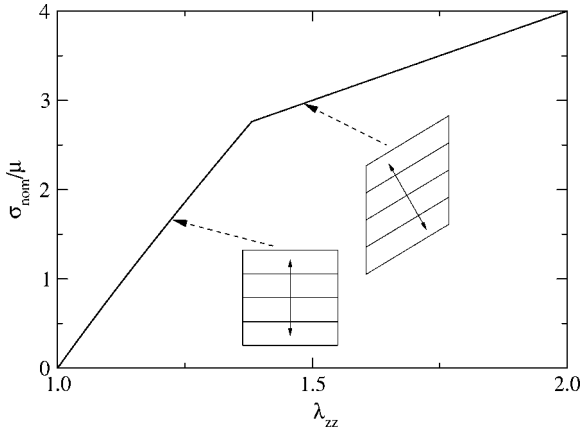

FIG. 4. Nominal stress for a smectic elastomer stretched parallel to the layer normal, with $r=2$ and $b=5$.

The specific forms given for the layer spacing and director are for the choice $\mathbf{n}_0=\mathbf{z}$ initially, as depicted in Fig. 1, which is useful for illustration; the coordinate-free forms given are of complete generality.

A. Imposed strain λ_{zz}

In this case, Fig. 1(a), the deformation tensor

$$\underline{\underline{\lambda}} = \begin{pmatrix} \lambda_{xx} & 0 & 0 \\ 0 & \lambda_{yy} & 0 \\ \lambda_{zx} & 0 & \lambda \end{pmatrix} \tag{11}$$

allows for the shear λ_{zx} which is an alternative means of increasing the z-dimension of the solid by layer rotation rather than layer dilation. This is the CMHH mechanism for elongation along the layer normal in smectics. The shear λ_{xz} in the presence of a z-force of extension would lead to torques and is not observed in smectics elastomers [1] or in the analogous nematic elastomer geometries that involve simultaneous director rotation and shear [12]. The volume constraint, layer spacing change, and director become, respectively,

$$1 = \lambda_{xx}\lambda_{yy}\lambda, \tag{12}$$

$$d/d_0 = 1/\left(\lambda_{yy}\sqrt{\lambda_{xx}^2+\lambda_{zx}^2}\right), \tag{13}$$

$$\mathbf{n} = \left(-\frac{\lambda_{zx}}{\sqrt{\lambda_{xx}^2+\lambda_{zx}^2}}, 0, \frac{\lambda_{xx}}{\sqrt{\lambda_{xx}^2+\lambda_{zx}^2}}\right). \tag{14}$$

The free energy density is then

$$f = \frac{1}{2}\mu\left[\lambda_{xx}^2 + \frac{1}{\lambda_{xx}^2\lambda^2} + \lambda_{zx}^2 + \frac{(\lambda_{xx}^2 + r\lambda_{zx}^2)\lambda^2}{\lambda_{xx}^2+\lambda_{zx}^2} + b\left(\lambda\lambda_{xx}/\sqrt{\lambda_{xx}^2+\lambda_{zx}^2} - 1\right)^2\right], \tag{15}$$

where volume conservation eliminates λ_{yy}.

Minimizing the free energy fixes the relaxing components of the deformation tensor for a particular b value; they are shown in Fig. 3. There is a critical, threshold value of the elongation $\lambda=\lambda_{cr}$ when the layer rotation starts to occur. The threshold will be shown to be a material property depending only upon b and r. The rather large threshold chosen for illustration arises from the small relative modulus, b, that has been adopted. The threshold is to a uniform state [given by Eq. (11)], see the sketch included in Fig. 4, and hence even exists independently of clamp constraints and microstructure which arise in practical cases, see Sec. IV D. Thus Frank elasticity has not yet been invoked for the threshold and will turn out to be largely irrelevant.

Shear λ_{zx} starts with a singular edge at the threshold and the transverse contraction λ_{yy} thereafter remains constant. The accompanying stress also divides into two distinct regimes with a much higher modulus before than after the transition, see Fig. 4. The layer rotation, given by **n**, Eq. (14), has the same singular edge and is plotted against $\lambda-1$ in Fig. 5 which also compares the calculated variation of orientation of the director with strain from the experiment of Nishikawa and Finkelmann [1]. The geometric reason why (cheap) shear does not immediately start, but only onsets after a threshold, is explained in Sec. III E 1.

Analytically, the solution to this model splits into two parts: before and after the discontinuity. Before the layers

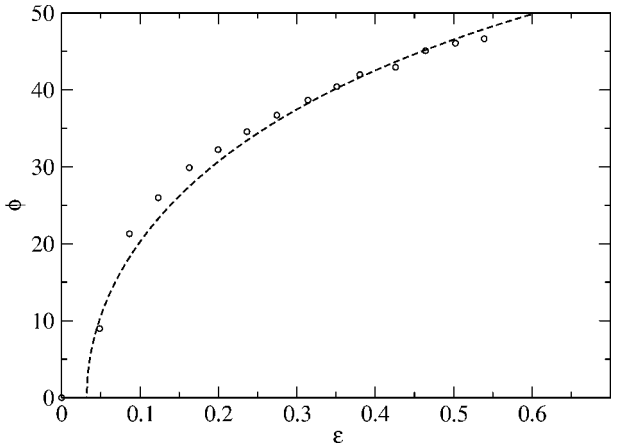

FIG. 5. Comparison of the calculated orientation of the director (dotted line) with the experimental points of [1] (circular points).

start to rotate, $\lambda_{zx}=0$. The free energy density is given by

$$f=\frac{1}{2}\mu\left(\lambda_{xx}^2+\frac{1}{\lambda_{xx}^2\lambda^2}+\lambda^2+b(\lambda-1)^2\right), \tag{16}$$

and has a minimum when $\lambda_{xx}^2=\lambda_{yy}^2=1/\lambda$. Thus before the layers start to rotate the two perpendicular directions are equivalent and the material has Poisson ratios $\left(\frac{1}{2},\frac{1}{2}\right)$ in the (x,y) directions. The free energy and the nominal stress, $\sigma_{\rm nom}=\partial f/\partial\lambda$, are

$$f=\frac{1}{2}\mu\left(\frac{2}{\lambda}+\lambda^2+b(\lambda-1)^2\right), \tag{17}$$

$$\sigma_{\rm nom}=\mu\left[\left(\lambda-\frac{1}{\lambda^2}\right)+b(\lambda-1)\right]. \tag{18}$$

Layer rotation starts at $\lambda_{\rm cr}$. Numerically it is clear that $\lambda_{yy}=1/\sqrt{\lambda_{\rm cr}}$ is a constant. With this assumption (to be confirmed below) after the transition, volume conservation then requires $\lambda_{xx}=\sqrt{\lambda_{\rm cr}}/\lambda$. If deformations were small, then one could say that the material now has Poisson ratios (1,0), to which we return when comparing with experiment.

If we minimize the free energy w.r.t. λ_{zx}^2 then, after some simplification, we obtain the condition

$$0=1+\frac{(r-1)\lambda^4\lambda_{\rm cr}}{(\lambda_{\rm cr}+\lambda_{zx}^2\lambda^2)^2}+b\left(\frac{\lambda^3\sqrt{\lambda_{\rm cr}}}{(\lambda_{\rm cr}+\lambda_{zx}^2\lambda^2)^{3/2}}-\frac{\lambda_{\rm cr}\lambda^4}{(\lambda_{\rm cr}+\lambda_{zx}^2\lambda^2)^2}\right). \tag{19}$$

The shear λ_{zx} only appears in the following combination

$$p^2=\lambda_{zx}^2+\frac{\lambda_{\rm cr}}{\lambda^2} \tag{20}$$

which is a function only of $r-1$, b and $\lambda_{\rm cr}$, that is $p(r,b,\lambda_{\rm cr})$, and obeys the equation

$$0=p^4+(r-1)\lambda_{\rm cr}+b(p\sqrt{\lambda_{\rm cr}}-\lambda_{\rm cr}). \tag{21}$$

p is not a function of λ and thus it can be fixed at any convenient value of λ. For instance at the critical extension $\lambda_{\rm cr}$, we have $\lambda_{zx}=0$ and hence $p=1/\sqrt{\lambda_{\rm cr}}$. The induced shear derives from putting this p into Eq. (20). The contractions and shears after the instability are then

$$\lambda_{xx}=\sqrt{\lambda_{\rm cr}}/\lambda,\quad \lambda_{yy}=1/\sqrt{\lambda_{\rm cr}}, \tag{22}$$

$$\lambda_{zx}=\pm\sqrt{\frac{1}{\lambda_{\rm cr}}-\frac{\lambda_{\rm cr}}{\lambda^2}}. \tag{23}$$

The shear displays the singular edge seen in Fig. 3. Both signs of shear give the same dilation along z at constant layer spacing. Both shears, and indeed all directions perpendicular to z (not just x), are required in a description of any induced microstructure (see Sec. IV C where this issue arises experimentally).

The director (and thus layer) rotation can be derived from the explicit expression (14) for **n**. For instance the first component gives

$$\sin\phi=\sqrt{1-(\lambda_{\rm cr}/\lambda)^2}, \tag{24}$$

which has the singular edge and distinctive form shown in Fig. 5 and in experiment.

Setting $p=1/\sqrt{\lambda_{\rm cr}}$ in Eq. (21) gives a cubic equation for $\lambda_{\rm cr}$

$$\lambda_{\rm cr}^3(r-b-1)+b\lambda_{\rm cr}^2+1=0. \tag{25}$$

To obtain a threshold at all we require $b>r-1$. Below this reduced layer modulus there is no instability—layer dilation is not significantly more costly than matrix distortion and it is no longer avoided by the intercession of an instability.

Instead of solving Eq. (25) analytically, it is more useful to analyze it in the physically important large b limit. The first few terms in an expansion yield the variation of critical extension with layer modulus

$$\lambda_{\rm cr}=1+\frac{r}{b}+r(r-3)\frac{1}{b^2}+O\left(\frac{1}{b^3}\right). \tag{26}$$

The choice of r and b in Figs. 3 and 4 is clearly outside the asymptotic realm of Eq. (26) but allows for an exaggerated clarity in Fig. 3.

The threshold behavior shown here occurs even for very small values of B down to $(r-1)\mu$. This is because the way in which the director deforms with the matrix has been imposed. Physically this is correct for large B. As B is reduced this constraint will become less rigidly enforced and the crosslinks will be able to move through one layer to the next. Thus the threshold behavior predicted for very small B values ($\sim\mu$) is unlikely to be correct in practice. Except close to the Sm-A–N transition, experimentally one deals with large values of B.

All components of induced deformation and the rotation of layers depend solely on (the imposed) λ and (the observable) $\lambda_{\rm cr}$, not in any separate or detailed way on the smectic potential b or the anisotropy r. This very tightly constrains theory since there are no free parameters and requires all rotation-strain and relaxation-strain relations, Eqs. (22)–(24), to be universal for all systems.

To calculate the stress, we substitute λ_{zx} back into the free energy and obtain the closed form

$$f=\frac{1}{2}\mu\left(\frac{2}{\lambda_{\rm cr}}+\lambda_{\rm cr}^2+r(\lambda^2-\lambda_{\rm cr}^2)+b(\lambda_{\rm cr}-1)^2\right). \tag{27}$$

From Eqs. (17) and (27) the nominal stresses, are

$$\sigma_{\rm nom}=\begin{cases}\mu(\lambda-1/\lambda^2)+B(\lambda-1), & \lambda<\lambda_{\rm cr}\\ \mu r\lambda, & \lambda>\lambda_{\rm cr}.\end{cases} \tag{28}$$

Note that the continuity of the nominal stress with λ can be used to derive Eq. (25). From this result it is clear that the ratio of the two slopes is related to $\lambda_{\rm cr}$, which provides another stringent constraint on theory. Thus for large b we can calculate the two slopes and obtain

$$\frac{r\mu}{B} \approx \lambda_{cr} - 1. \tag{29}$$

Experimentally one could obtain μ from stretching the rubber in the layers, and thus obtain the anisotropy of the polymers, r. The large B/μ expression Eq. (29) for the threshold strain essentially agrees with the result of Weilepp and Brand [6] if one neglects Frank effects. These authors, and we in Sec. IV D, show that Frank elasticity has a small effect on the threshold strain but does influence the length scales of the subsequent microstructure. Reference [6] ignores the anisotropy of the underlying nematic network and thus the factor r is absent from their expression.

The layer spacing of the system as a function of the imposed stretch is

$$\frac{d}{d_0} = \frac{1}{\lambda_{yy}\sqrt{\lambda_{xx}^2 + \lambda_{zx}^2}} = \frac{\lambda\lambda_{xx}}{\sqrt{\lambda_{xx}^2 + \lambda_{zx}^2}}. \tag{30}$$

Before layer rotation starts $\lambda_{zx}=0$ and so the layer spacing increases as $d/d_0=\lambda$. After layer rotation starts we have, from the same expression, $d/d_0=\lambda_{cr}$; layer spacing remains fixed. The only cost in deforming the system is that of shearing the rubber. This is because, as the layers rotate, the component of the force along the layers remains constant. Furthermore, because shear (as opposed to extension and contraction along principal directions) involves the chain anisotropy and it is the cost of this shear that is to be compared with that of layer dilation, we can understand that r (as well as the relative modulus b) enters the expression for λ_{cr}.

We check that there are no other solutions by writing the free energy as a function of the two variables λ_{xx} and $\tan\phi = -\lambda_{zx}/\lambda_{xx}$ and without making any assumptions about $\lambda_{yy}(\equiv 1/\lambda_{xx}\lambda)$

$$f = \frac{1}{2}\mu\left[\lambda_{xx}^2 + \frac{1}{\lambda_{xx}^2\lambda^2} + \lambda_{xx}^2\tan^2\phi + (\cos^2\phi + r\sin^2\phi)\lambda^2 + b(\lambda\cos\phi - 1)^2\right]. \tag{31}$$

Minimizing with respect to λ_{xx} we obtain

$$0 = 2\lambda_{xx}\left(1 - \frac{1}{\lambda^2\lambda_{xx}^4} + \tan^2\phi\right) \tag{32}$$

with solutions $\lambda_{xx}^2=0, \pm(\cos\phi)/\lambda$. The only physical solution is $\lambda_{xx}^2=\cos\phi/\lambda$. Minimizing the free energy with respect to ϕ and substituting for λ_{xx} yields

$$0 = \frac{\sin\phi}{\lambda\cos^2\phi} + \lambda^2(r-1)\sin\phi\cos\phi - b\lambda(\lambda\sin\phi\cos\phi - \sin\phi)$$

which can be factorized

$$0 = \lambda\sin\phi\left(\cos\phi - \frac{\lambda_{cr}}{\lambda}\right) \times \left(\lambda^2(r-1-b)\cos^2\phi - \frac{\lambda}{\lambda_{cr}^2}\cos\phi - \frac{1}{\lambda_{cr}}\right) \tag{33}$$

provided that Eq. (25) is obeyed. Thus our solution (a combination of the first and second factors) was a minimum. The third factor is real only if $\lambda_{cr}^2 b < -3/4$ and therefore never relevant; thus the minimum was unique.

B. Imposed λ_{xx}

We consider the deformation gradient matrix

$$\underline{\underline{\lambda}} = \begin{pmatrix} \lambda & 0 & \lambda_{xz} \\ 0 & \lambda_{yy} & 0 \\ 0 & 0 & \lambda_{zz} \end{pmatrix}. \tag{34}$$

Volume conservation is simply expressed by

$$1 = \lambda\lambda_{yy}\lambda_{zz} \tag{35}$$

because the matrix is upper triangular. The layer spacing and director are now given by: $d/d_0=1/(\lambda_{yy}\lambda)$ and $\mathbf{n}=(0,0,1)$. Intuitively such imposed extensions should not rotate the layers since a cheap, volume-conserving response is simply to contract along y leaving the more expensive z dimension unchanged. This is one reason why we have not included shear λ_{zx} since from the form of the new director (layer normal), Eq. (14), it is precisely this shear that induces layer rotation. Moreover, this shear also introduces torques from the change of shape in the presence of an x component of force which tends to eliminate the distortion. The conclusion of this section is also that the other component of shear vanishes too, which we confirm directly.

The deformation tensor substituted into the free energy, and the volume conservation constraint eliminating λ_{zz}, results in

$$f = \frac{1}{2}\mu\left[\lambda_{yy}^2 + r\lambda_{xz}^2 + \lambda^2 + \frac{1}{\lambda_{yy}^2\lambda^2} + b\left(\frac{1}{\lambda_{yy}\lambda} - 1\right)^2\right]. \tag{36}$$

The shear only appears once, hence minimization yields $\lambda_{xz}=0$. Minimization of this free energy with respect to λ_{yy} gives

$$\lambda^2\lambda_{yy}^4 - 1 = b(1 - \lambda\lambda_{yy}). \tag{37}$$

From this equation it is clear that the limits of small and large b correspond to $\lambda_{yy}=1/\lambda$ (with $\lambda_{zz}=1$) and $\lambda_{yy}=\lambda_{zz}=1/\sqrt{\lambda}$, respectively. The material with a small b value is still a Sm-A in the sense that the director is constrained to lie along the layer normal. To calculate the Poisson ratios from this expression we make the small strain expansions

$$\lambda_{yy} = 1 + \epsilon, \tag{38}$$

$$\lambda = 1 + \omega, \tag{39}$$

when to first order in ω and ϵ, Eq. (37) becomes

$$4\epsilon + 2\omega + b(\epsilon + \omega) = 0. \tag{40}$$

The Poisson ratio in the y direction, $\nu_y = -\epsilon/\omega$, and that in the layer direction, ν_z are

$$\nu_y = \frac{2+b}{4+b}, \quad \nu_z = \frac{2}{4+b}. \tag{41}$$

The crossover from Poisson ratios $(z,y)=(0,1)$ to $(1/2, 1/2)$ is thus relatively slow. However, it is clear that for $b \sim 60$, as found [1] in some experimental samples, the material is firmly in the (0,1) class.

For large b where layer relaxation is suppressed ($\lambda_{zz} \to 1$), the elastomer is like a classical 2D rubber. Since there is no director rotation, r does not enter. The free energy density (36) reduces to

$$f = \frac{1}{2}\mu\{\lambda^2 + \lambda_{yy}^2\} = \frac{1}{2}\mu\{\lambda^2 + 1/\lambda^2\} \tag{42}$$

as a consequence of higher layer stiffness and volume conservation. The Young's modulus derived from Eq. (42) is $E_\perp = \partial^2 f/\partial\lambda^2|_{\lambda=1} = 4\mu$, rather than the value 3μ that obtains for a 3D rubber. Dimensional constraints have increased the modulus. However this must remain an upper bound on $E_\perp$ for reasons we discuss in Sec. IV B.

C. Imposed λ_{xz}

Consider the deformation gradient matrix

$$\underline{\underline{\lambda}} = \begin{pmatrix} \lambda_{xx} & 0 & \lambda \\ 0 & \lambda_{yy} & 0 \\ 0 & 0 & \lambda_{zz} \end{pmatrix}. \tag{43}$$

We suppress λ_{zx} since typically the application of λ_{xz} is with plates that constrain the sample. Again, volume conservation is simply expressed by

$$1 = \lambda_{xx}\lambda_{yy}\lambda_{zz}. \tag{44}$$

We eliminate λ_{yy} by using the volume conservation constraint. The resulting free energy is

$$f = \frac{1}{2}\mu\left(\lambda_{xx}^2 + \frac{1}{\lambda_{xx}^2\lambda_{zz}^2} + \lambda_{zz}^2 + r\lambda^2 + b(\lambda_{zz}-1)^2\right). \tag{45}$$

The shears λ and λ_{zz} do not couple and so the imposed shear cannot affect λ_{zz}. Minimizing over λ_{xx} and λ_{zz} yields $\lambda_{zz} = \lambda_{xx} = 1$ and the free energy density becomes

$$f = \frac{1}{2}\mu\{3 + r\lambda^2\}. \tag{46}$$

The result is for simple shear in a nematic elastomer with unrotating director. The anisotropy enters in the classical way—for large r the effective modulus $r\mu$ becomes large because chains extend across several shear planes. This modulus is identical to that obtained after the instability on stretching along the layer normal, Eq. (28), because then deformation is largely via shears in the rotated planes.

D. Imposed λ_{zx}

Consider imposing the deformation in Fig. 1(d)

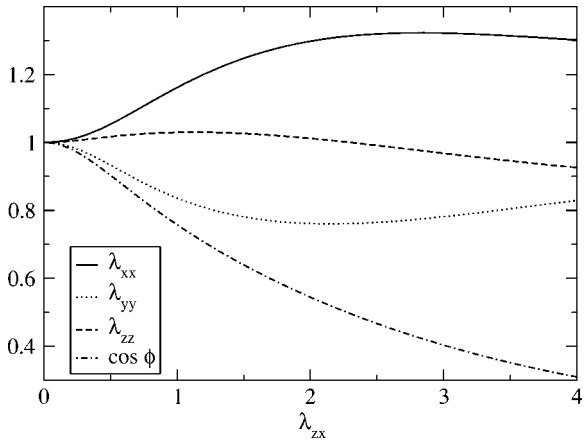

FIG. 6. Relaxing components of the deformation tensor on imposing λ_{zx} for a rubber with $b=5$, $r=3$.

$$\underline{\underline{\lambda}} = \begin{pmatrix} \lambda_{xx} & 0 & 0 \\ 0 & \lambda_{yy} & 0 \\ \lambda & 0 & \lambda_{zz} \end{pmatrix}. \tag{47}$$

It is lower triangular. Allowing a λ_{xz} component causes the elastomer to simply rotate 90° and experience an effectively pure λ_{xz} deformation. The director and volume conservation are given by

$$\mathbf{n} = \frac{1}{\sqrt{\lambda^2 + \lambda_{xx}^2}}(-\lambda, 0, \lambda_{xx}), \tag{48}$$

$$1 = \lambda_{xx}\lambda_{yy}\lambda_{zz}. \tag{49}$$

On eliminating λ_{yy} by volume conservation, the free energy density is

$$f = \frac{1}{2}\mu\left[\lambda_{xx}^2 + \frac{1}{\lambda_{xx}^2\lambda_{zz}^2} + \lambda^2 + r\lambda_{zz}^2 + \frac{\lambda_{zz}^2(\lambda_{xx}^2 + r\lambda^2)}{\lambda_{xx}^2 + \lambda^2} + b\left(\frac{\lambda_{xx}\lambda_{zz}}{\sqrt{\lambda_{xx}^2 + \lambda^2}} - 1\right)^2\right], \tag{50}$$

which can be numerically minimized using the simplex algorithm. A typical solution is illustrated in Fig. 6. Figure 7 shows the corresponding layer spacing change for imposed λ_{zx}. In this deformation we are thus effectively compressing the layers. Even for very large b, the layer spacing eventually yields and begins to decrease.

E. General decomposition of shear

Deformations can be decomposed into a minimal set of three component deformations, an imposed λ_{xx}, λ_{xz}, and λ_{zz}, plus a rotation. The choice is natural since λ_{zz} by itself can describe a layer compression or extension, λ_{xx} along with constancy of volume can describe shape changes of the smectic layers and λ_{xz} describes out of plane shears at constant layer spacing. We return shortly to the significance of the latter when we explain how the threshold to instability under imposed λ_{zz} arises.

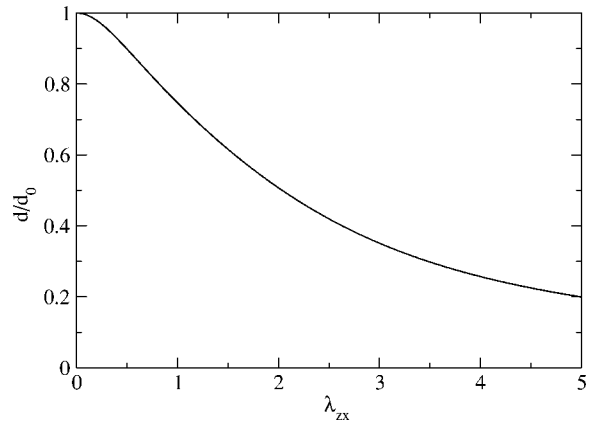

FIG. 7. Relative layer spacing change on imposing λ_{zx} for the rubber of Fig. 6.

As an example we decompose the λ_{zx} deformation. It is nontrivial since, as we have seen this shear induces a layer compression. It is broken up into

$$\underline{\underline{\lambda}} = \underline{\underline{W}} \cdot \underline{\underline{D}}, \tag{51}$$

where rotation and deformation of the solid matrix are

$$\underline{\underline{W}} = \begin{pmatrix} \cos\gamma & 0 & \sin\gamma \\ 0 & 1 & 0 \\ -\sin\gamma & 0 & \cos\gamma \end{pmatrix}$$

$$\underline{\underline{D}} = \begin{pmatrix} 1 & 0 & \lambda_{xz} \\ 0 & 1 & 0 \\ 0 & 0 & 1 \end{pmatrix} \begin{pmatrix} \lambda_{xx} & 0 & 0 \\ 0 & \dfrac{1}{\lambda_{zz}\lambda_{xx}} & 0 \\ 0 & 0 & \dfrac{1}{\lambda_{zz}} \end{pmatrix}.$$

The layer stretch and in-plane deformation is followed by a λ_{xz} shear, which is then followed by a rotation. Overall, the deformation gradient tensor is thus

$$\underline{\underline{\lambda}} = \begin{pmatrix} \lambda_{xx}\cos\gamma & 0 & \lambda_{zz}(\lambda_{xz}\cos\gamma + \sin\gamma) \\ 0 & \dfrac{1}{\lambda_{xx}\lambda_{zz}} & 0 \\ -\lambda_{xx}\sin\gamma & 0 & \lambda_{zz}(\cos\gamma - \lambda_{xz}\sin\gamma) \end{pmatrix}. \tag{52}$$

From this deformation we can calculate the director

$$\underline{\underline{\lambda}}^{-T} \cdot \mathbf{n}_0 = \left(\frac{\sin\gamma}{\lambda_{zz}}, 0, \frac{\cos\gamma}{\lambda_{zz}} \right) \rightarrow (\sin\gamma, 0, \cos\gamma), \tag{53}$$

where the final expression is the normalized director. The rotation required to reduce this deformation to the form of an imposed λ_{zx} deformation is $\tan\gamma = -\lambda_{xz}$ which is what eliminates the upper right element of $\underline{\underline{\lambda}}$. Then,

$$\underline{\underline{\lambda}} = \begin{pmatrix} \alpha & 0 & 0 \\ 0 & \dfrac{1}{\alpha\beta} & 0 \\ \lambda & 0 & \beta \end{pmatrix}, \tag{54}$$

where

$$\alpha = \sqrt{\lambda_{xx}^2 - \lambda^2}, \quad \beta = \frac{\lambda_{xx}\lambda_{zz}}{\sqrt{\lambda_{xx}^2 - \lambda^2}}, \quad \lambda = \frac{\lambda_{xx}\lambda_{xz}}{\sqrt{1 + \lambda_{xz}^2}}.$$

Since the deformation (54) is now of the same form as our simple starting point Eq. (47), the free energy is then of the same form as Eq. (50) and we have the decomposition of the mode. This decomposition is significant because it shows that there are only three different deformations that the sample can undergo once we have removed a trivial rotation. This is dramatically different from the case of nematic elastomers.

1. The geometrical basis of the CMHH instability

If shears are cheaper than layer dilations by a factor of $1/b = \mu/B$ why is there a threshold at all for the CMHH deformations in response to an imposed λ_{zz}? At first sight Eq. (11) and Fig. 4 would seem to suggest that there is simply a λ_{zx} shear after the instability. In this frame, this is indeed true but it is clearly accompanied by other distortions required to keep the layer spacing constant (see the insets in Fig. 4). A λ_{zx} shear alone causes the layer spacing to contract.

A decomposition can be performed on the imposed λ_{zz} deformation. In this case we start from Eq. (52) and set $\tan\gamma = -\lambda_{xz}$. We can then identify $\lambda = \lambda_{zz}\sqrt{1+\lambda_{xz}^2}$. This decomposition gives a geometric reason for the threshold. Suppose that the elastomer deforms with only the λ_{zz} component. The free energy density is then

$$f_{zz} = \tfrac{1}{2}B(\lambda - 1)^2. \tag{55}$$

Alternatively the sample could deform by a shear λ_{xz}, which leaves the layer spacing unchanged, and then rotate to accomplish the same λ_{zz} value. In this case the free energy density is

$$f_{xz} = \tfrac{1}{2}\mu r\lambda_{xz}^2 = \tfrac{1}{2}\mu r(\lambda^2 - 1). \tag{56}$$

Comparing these two energies for small ϵ where $\lambda = 1 + \epsilon$, we find that $f_{zz} \sim \frac{1}{2}B\epsilon^2 < f_{xz} \sim \mu r\epsilon$, provided that $\epsilon < 2\mu r/B$. The latter energy is first order rather than second order in the strain and explains why it is so costly and unphysical (it is second order finally where it intercedes after λ_{cr}. This decomposition also shows that an imposed λ_{zz} is equivalent to an imposed λ_{xz} deformation plus a rotation and a *fixed* stretch along the layer normal such that $d/d_0 = \lambda_{cr}$). The decomposition explains why the modulus of the sample after the threshold is the same as that for an imposed λ_{xz} deformation.

IV. COMPARISON WITH EXPERIMENT

Three different types of experiments have yielded information on the response of Sm-*A* elastomers–strain response, stress–strain, and rotation–strain measurements. We calculate

detailed results in all these areas and now compare with the relevant experiments of Nishikawa and Finkelmann [NF] [1], not only the functional forms of responses but also the interconnections between the physical variables entering our description, that is layer and shear moduli B and μ, chain anisotropy r, and threshold strain λ_{cr}. We focus here on the two strains imposed by NF, λ_{zz}, and λ_{xx}.

Our theory is not relevant to weakly coupled smectic elastomers where there is no elastic signature of the smectic layer system [13]. Such elastomers are apparently well-described by isotropic rubber elasticity as is appropriate for a nematic elastic matrix where the director cannot rotate (biaxial strains in the layer planes were examined).

A. Strain response

The Poisson ratio is a measure of transverse strain response at small strains. For imposed λ_{zz} the experimental response is isotropic and volume preserving, Poisson ratios $(1/2,1/2)$, until the layer instability is reached. Thereafter, the transverse relaxation is apparently $(1/\lambda^{1/2},1/\lambda^{1/2})$ from a close inspection of the snapshot of large strain given in Fig. 4 of NF. The authors do not give a functional dependence but the figure rules out the predicted monodomain post-threshold response Eq. (22) which, if strains were small would correspond to Poisson ratios (1,0). This discrepancy is not surprising given that there is clearly not a monodomain after λ_{cr}. We return to this question in our analysis of layer rotation and x-ray experiments.

Imposed in-plane stretches λ_{xx} give predicted Poisson ratios

$$(\nu_y,\nu_z)=\left(\frac{2+b}{4+b},\frac{2}{4+b}\right).$$

Experimentally NF give (1,0) corresponding to $b\gg 1$. These Poisson ratios agree with the stress results that show that smectic order is much more rigid than rubber elastic effects.

B. Stress

Figure 8 shows that nominal stress-strain $(\lambda-1)$ data of NF for imposed $\lambda=\lambda_{zz}$ along the initial layer normal direction. It is fitted to Eq. (28). From the data one can deduce that the ratio of the slopes is 4.1×10^{-2}. We predict in Eq. (28) this ratio should be $\mu r/B=r/b$ whereupon $b=r/4.1\times10^{-2}\gg1$ is evidently large. In the limit of such smectic moduli, Eq. (29) predicts the direct connection $r/b=\lambda_{cr}-1$ for the threshold giving here $\epsilon_{cr}=\lambda_{cr}-1\approx4\%$ which is extremely close to that observed in Fig. 8.

In-plane stress and moduli in response to imposed λ_{xx} were not reported by NF. The in-plane Young's modulus, $E_\perp$, is known from other work to comparable to the postthreshold modulus, E_{after} say. The in-plane Young's modulus was calculated in Sec. III B.

Many Sm-*A* elastomers that have been investigated are suspected to be de Vries phases, that is where there is incipient Sm-*C* ordering. This tilt is not long ranged in its order. The signature of this local order is that the transition to the Sm-*C* state with long ranged order is not accompanied by a layer spacing change as expected from the transition from a standard Sm-*A*. Applied strain λ_{xx} in one in-plane direction could extend the correlation in Sm-*C* ordering and direct it along the strain, allowing the rubber to extend along x at lower energy cost than 4μ. Tests of this type of response would be: (i) The observation of in-plane induced optical birefringence. While an untilting director remains anchored along the layer normal, the response should be that of a classical elastomer where stress induces very small birefringence compared with that in any liquid crystal system. In comparison a de Vries elastomer would have a huge birefringence response. (ii) The ratio $E_{after}/E_\perp$ is predicted to be $r\mu/4\mu=r/4$. Departures from this ratio could be due to a low $E_\perp$ because of de Vries. However to some extent de Vries should also intervene in E_{after} since there is an element of in-plane stretch in the now rotated planes. The balance between the intervention of de Vries effects in the two moduli is not trivial since the component of stretch in-plane and the degree of shear acting both change with strain beyond the threshold for the E_{after} case.

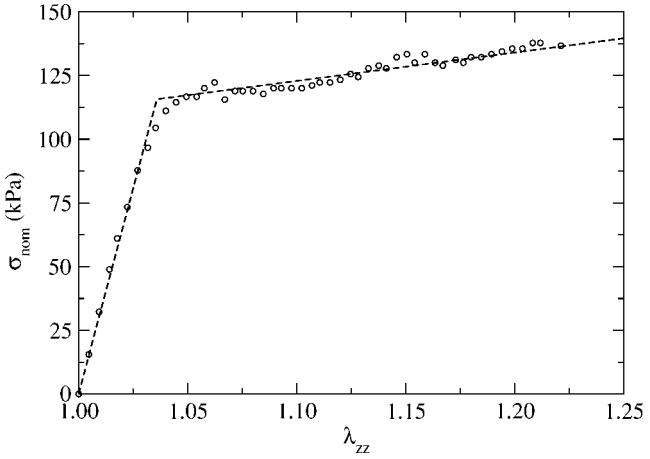

FIG. 8. Stress against imposed deformation λ_{zz} - solid line theory, points are data of Ref. [1]. Crossover occurs at a threshold strain of 4% as in Fig. 5.

C. Layer rotation and x-ray scattering

Layer rotation against strain starts in a singular manner at a threshold λ_{cr} both in theory, Eq. (24), and in an x-ray determination of layer orientation, Fig. 5. Agreement with $\phi(\lambda)$ is good, but a major problem of interpretation remains. As strain increases, the x-ray intensity associated with the rotating layer lines diminishes sharply. NF proposed that above λ_{cr} a diminishing fraction of the sample rotates while an increasing fraction melts to a nematic state. On energetic grounds this appears unlikely since the smectic energy scale is high compared with the rubber elastic scale. The entropy change found by NF for the smectic-isotropic phase transition was $\Delta S=2.4\times10^{-2}$ J K^{-1} g^{-1}. Thus the cost for melting at 300 K for a sample with density $\rho\sim1$ g cm^{-3} is $T\Delta S\rho\sim7.2\times10^6$ J m^{-3}. To pay the cost of melting, an energy density of $\frac{1}{2}B(\lambda_{cr}-1)^2\sim8\times10^4$ J/m^3 is available and is clearly rather small.

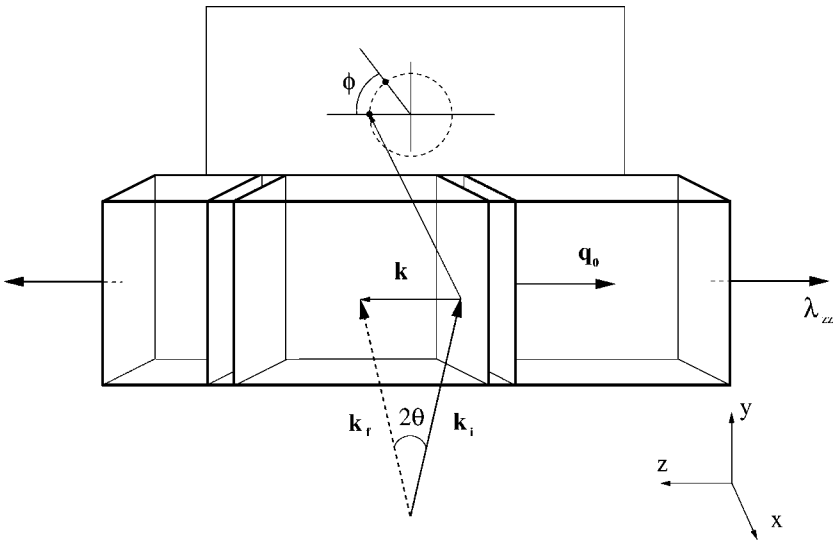

FIG. 9. The x-ray scattering setup. Layer normals are initially along the stretch direction *z*. The incoming beam is scattered through an angle 2θ having been incident at an angle θ. The final beam is detected on an image plate behind, on which a circle of spots is dotted for the cases where layers are rotated through angle ϕ. The scattering vector $\mathbf{k}$ is along the layer normal and for Bragg scattering matches the layer vector, initially $\mathbf{q}_0$.

A more direct explanation than melting is that layers rotate their normals towards all directions perpendicular to the stretch along the original layer normal $\mathbf{n}_0$. Section III A calculates the contraction and shear in the x direction perpendicular to original layer normal z [Eqs. (22) and (23)] and the rotation of the normal toward x [Eq. (24)], but no direction perpendicular to the original director is privileged (in contrast to stripe formation in nematic elastomers). We must consider all other axes perpendicular to $\mathbf{n}_0$. This breakup of the sample into a microstructure of regions of tilted domains is cylindrically symmetric around the stretch axis. The regions that are tilted toward the x-ray beam no longer meet the Bragg condition for diffraction, and as a result do not contribute intensity to the observed scattered beam. We suggest that the drop in x-ray intensity is simply a result of polydomain formation. Additionally, the overall Poisson ratios observed in the two, now equivalent directions perpendicular to the original layer normal are $(\frac{1}{2},\frac{1}{2})$ rather than the monodomain values (1,0).

A small angle setup is sketched in Fig. 9. Scattering in NF is through an angle 2θ where $2\theta \sim 3°$. For the shown incoming and final beams, $\mathbf{k}_i$ and $\mathbf{k}_f$, the scattering vector $\mathbf{k}=\mathbf{k}_f-\mathbf{k}_i$ is along the layer normal. Under these circumstances one can satisfy the Bragg condition:

$$\mathbf{k} = \mathbf{q}_0 \rightarrow \frac{4\pi \sin\theta}{\lambda_0} = \frac{2\pi}{d_0}, \tag{57}$$

where λ_0 is the x-ray wavelength and d_0 the layer spacing. This fixes the angle 2θ. The sketched setup is not quite that of NF since they direct the incident beam perpendicular to the sample, i.e., along the x-axis. This means that $\mathbf{k}$ is misaligned from the layer vector $\mathbf{q}_0$ and hence also from the Bragg condition by an angle θ. Line visibility before stretching occurred suggests that the intrinsic width of the lines is of order θ or more. Since θ is rather small, we continue analyzing Fig. 9 rather than that of NF.

Consider planes rotated clockwise by ϕ about x so that their normals remain in the (y,z) plane and make an angle ϕ with the stretch direction z. Clearly then the scattering plane which includes $\mathbf{k}$, $\mathbf{k}_i$, $\mathbf{k}_f$, and $\mathbf{q}_0$ also rotates by ϕ and the layer spot rotates on the image plate to the position indicated by ϕ. Planes performing this rotation retain a satisfiable Bragg condition and are those seen in experiment. Polydomain layer normal arrangements would have planes with normals forming angle ϕ with the z axis but randomly distributed in their azimuthal angle α about z, the circle in Fig. 10 which gives the sphere of radius $|\mathbf{q}|=2\pi/d_0$ where the layer vectors $\mathbf{q}$ can sit. Only those planes with a $\mathbf{q}$ that matches a $\mathbf{k}$ in the (y,z) plane to within their natural angular width δ_c can contribute to the scattering. In Fig. 10 a plane vector and its natural width are shown. Its angle α for this ϕ is clearly sufficiently large enough to remove overlap with the scattering vector. The contributory fraction of the plane normals rapidly diminishes as ϕ initially increases. The angular separation, δ, of $\mathbf{k}$ and the $\mathbf{q}$ at α is $\sin(\delta/2)=\sin\phi\sin(\alpha/2)$. Only sets of planes with $\mathbf{q}$ such that their α angles give a separation $\delta<\delta_c/2$ from $\mathbf{k}$ will contribute to the scattering. The critical azimuthal separation α_c is given by

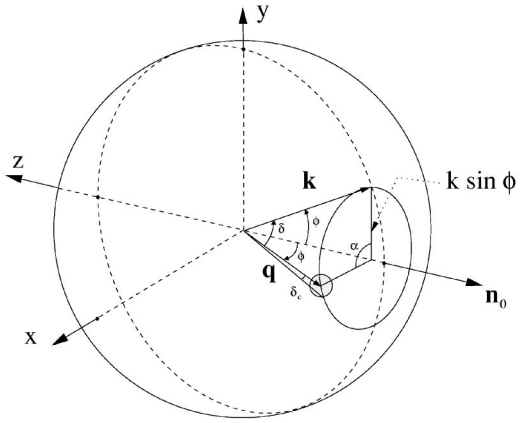

FIG. 10. The spherical shell of layer vectors $\mathbf{q}$. Those with angle ϕ sit on a circle centered about the initial layer normal $\mathbf{n}_0$. A $\mathbf{q}$ vector is at angle δ with respect to a scattering vector $\mathbf{k}$ in the (y,z) plane.

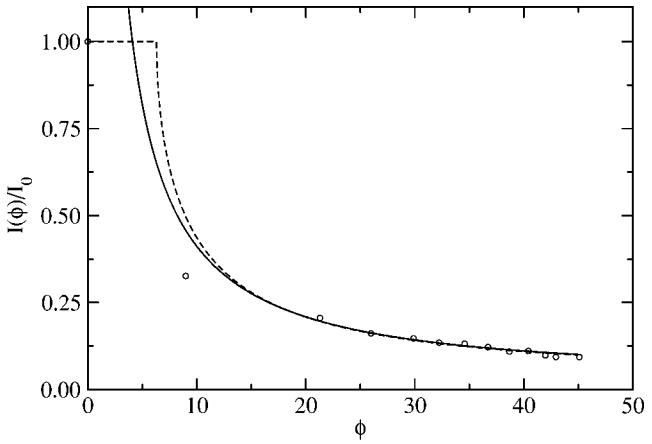

FIG. 11. The experimental data (○) of [1]. The solid curve corresponds to $0.3/\sin\phi$ which ignores the intrinsic width of layer lines; the dashed curve is $(2/\pi)\sin^{-1}(0.1045/\sin\phi)$ which accounts for linewidth.

$$\sin(\alpha_c/2) = \sin(\delta_c/2)/\sin\phi, \tag{58}$$

that is, plane normals in the interval $-\alpha_c < \alpha < \alpha_c$ will have lines overlapping with **k** and thus contribute to the x-ray intensity. As $\phi \to 0$, the circle of **q** at ϕ is so small that all planes irrespective of their position α on the circle contribute to the scattering. This is clearly when $\phi = \delta_c/2$ and indeed the condition (58) gives $\sin\alpha_c/2 = 1$ or $\alpha_c = \pi$ and all domains contribute. The intensity for $\phi > \delta_c/2$ is then

$$I(\phi) = I_0 \frac{2\alpha_c}{2\pi} = I_0 \frac{2}{\pi} \sin^{-1}\left(\frac{\sin(\delta_c/2)}{\sin\phi}\right), \tag{59}$$

where the first factor stresses that a fraction $2\alpha_c/2\pi$ of all possible sets of planes contributes. The sharp switch from the $I(\phi)$ above to the saturated value I_0 for $\phi < \delta_c/2$ is a consequence of our artificial assumption that planes either overlap with the detector or not, rather than gradually losing their overlap. The intensity variation $I(\phi)/I_0$ is shown in Fig. 11. There is qualitative agreement with the NF experimental points that are shown.

Several problems comparing with data arise. No $I(\phi)$ plot was directly available to us: the data were abstracted from $\phi(\epsilon)$ and $I(\epsilon)$ plots given by NF. The first data point for $\phi \neq 0$ carries the highest burden of error since it is taken from a $\phi(\epsilon)$ plot of seemingly infinite gradient around ϵ_c. Second, the lines at small ϕ especially were conspicuously asymmetric between $\pm\phi$. Is the attribution of intensity to $I(\phi)$ ambiguous as a result? In any event it is evident from the data that a very rapid drop in intensity from $\phi = 0$ takes place. The residual small angle (in θ) intensity about $\phi = 0$, that is representing unrotated layer systems, is relatively much more constant with strain. It is initially a very small fraction of the rotated layer line intensity but increases in relative importance because the layer lines diminish so quickly. It may represent regions near the boundaries of the elastomer or near clamps. These planes rotate much later than the bulk (which is consistent with the contribution finally diminishing with strain). Such heterogeneity in rotation is well known in the quasiconvexification of nematic elastomer response by the creation of polydomains [14]. The effect of having a distribution of **q** vectors with random α on the large angle scattering (and hence on the perceived nematic order parameter) is more complicated and we return to that elsewhere.

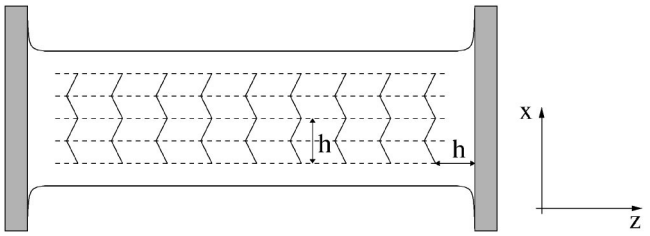

FIG. 12. The microstructure of a sample loaded past the threshold stress. Stripes (dotted) of width h are shown coarsened, the layer normals being at $\pm\phi$ with respect to the extension axis, z.

D. Microstructure after the CMHH transition

When elongation along the layer normal, λ_{zz} becomes too costly we have seen that layers rotate instead of dilating further (Fig. 4). However, the sample must be clamped in order to apply a z-extensional force and thus the rotation cannot occur uniformly throughout the sample. It must vanish at $z = 0$ and $z = L_z$, that is at the clamps, and must vary in the x direction between the values $\pm\phi$, Eq. (24), sufficiently rapidly that large layer translations are not built up which would then cost large elastic energies to satisfy the clamp constraints, see Fig. 12. On the other hand, very fast x variation between $\pm\phi$ leads to a high Frank elastic energy cost. The resulting x-length scale and overall energy cost arises from optimizing the sum of these two energies. Microstructure development in layered systems with disparate moduli is a classic problem in liquids [2]. It also occurs in thermoplastic elastomers and in a wide variety of other layered materials [15]. Here we give a short analysis to produce a first estimate.

Length scales emerge naturally from layer and matrix elastic moduli B and μ competing with Frank elastic energies which, for simplicity, we represent by a single constant κ. One obtains geometric quotients from Euler-Lagrange analysis: $\xi = \sqrt{\kappa/\mu} \sim 10^{-8}$ m for the nematic penetration depth. It is a measure of how deeply a director variation can penetrate into the depth of a material while acting against the penalty for director rotation. It determines stripe interfacial lengths and the seemingly instant coarsening in the analogous strain-induced microstructure observed in nematic elastomers [12]. Analogously, one defines the usual smectic penetration depth $\xi_{sm} = \sqrt{\kappa/B} \simeq d_0 \sim 10^{-9}$ m which determines the penetration of distortion into a smectic structure. It is independent of the rubbery elasticity and is an even smaller length suggesting that smectic microstructure should also be instantly coarsened. The geometric mean of the smectic and Frank scales gives an interfacial energy density for the energy cost per unit area of stripe formation—$\gamma_{sm} = \sqrt{\kappa B}$.

One finds, in close analogy to the nematic stripes problem [12], that the threshold $\lambda_{zz} = \lambda_{cr}$ found in the case of instability to a uniform system is shifted very slightly by Frank

effects to a higher $\lambda'_{cr} \geq \lambda_{cr}$ at which point there is a small jump to a finite $\phi > 0$. The creation of microstructure to accommodate clamp constraints means there are spatial variations and thus a (small) Frank contribution to the energy. A little more strain must be imposed to overcome this additional cost.

The stripe period in the x direction is

$$h \sim \sqrt{L_z \xi_{sm} B/(r\mu)} \frac{1}{(\lambda - \lambda_{cr})^{1/4}}. \tag{60}$$

The period never diverges since $\lambda \geq \lambda'_{cr} \geq \lambda_{cr}$ and rapidly saturates to

$$h \sim \sqrt{L_z \xi_{sm} B/(r\mu)} \sim \sqrt{10^{-3} \times 10^{-9} \times 20}\ \text{m} \sim 4\ \mu\text{m},$$

for a sample of length $L_z \sim 10^{-3}$ m. This is in the scale of lengths which would give the strong light scattering that is actually observed. Microscopic results for h are not yet available as they are in the nematic case. It would be interesting to investigate stresses and rotations the threshold region in detail, and to examine stripes in a microscope.

V. MATRIX-LAYER COUPLING FROM CROSSLINK LOCALIZATION

We derive the underlying rubber elasticity and the rigid layer-matrix constraints for a smectic elastomer where network crosslinks are strongly coupled to smectic order. However, there is still disagreement in this still-controversial area as to how this coupling comes about. One argument for their being no constraint on layer motion relative to the rubber matrix has been advanced by Radzihovsky [16]. It rests on the statistical spatial homogeneity of crosslink positions in a network crosslinked in the nonsmectic state (most probably the case of NF). On then entering the smectic state-chain spans stretch or compress during the sinking of their crosslinked ends into the smectic potential minima. Such homogeneity means that the energy in the smectic state is independent of where the layers form relative to the rubber matrix. Given all positions of the layer system have identical energy, there should be no modulus governing the position of layers relative to the matrix. A similar argument [9,10] can be constructed in the orientational case for soft elasticity in nematic elastomers. An isotropic (here, layer-free) gedanken state is required (to establish the energetic equivalent of differing states).

We believe that despite the independence of energy on layer position, there is indeed resistance to layer displacement relative to the matrix if crosslinks sink into sufficiently deep minima in the smectic potential. An equilibrium layer system displaced from a given system, after being heated to and then cooled from the nonsmectic gedanken state, will have the same energy. However, given strands may end in different minima in the two systems but on displacing the original layer system at fixed temperature, chains may not reach their minima appropriate to the translated layer system because of smectic localization, and then the energy must indeed rise. We now calculate this energetic cost in the limit of strong order. The harmonic coupling constant Λ, introduced in [3] for layer-matrix relative translations, will emerge explicitly as will the rigid constraints on matrix shear relative to layer rotation, Eqs. (3) and (4). As the Sm-*A* to nematic transition is approached from below, one would expect the rigid coupling to be lost and a crossover from 2D to 3D rubber elasticity to occur.

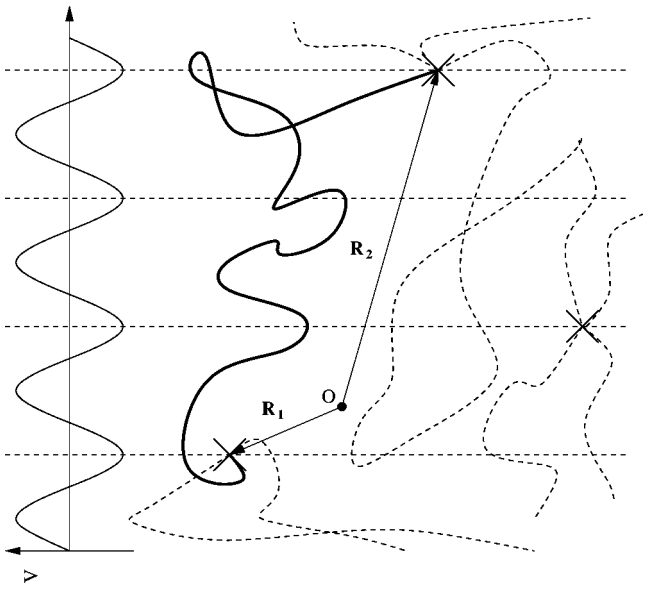

FIG. 13. A microscopic model of a smectic elastomer. Crosslink points sit in a periodic potential resulting from the smectic ordering. For clarity, the smectogens are not shown.

Microscopic models of ordinary and nematic elastomers require the probability distribution of end-to-end spans of the network polymers. The trace formula (6) derives from the averaged logarithm of the distribution, that is of the partition function conditional on fixed end-to-end distance. For a smectic elastomer both the size of the span of a polymer chain and additionally the position of its ends relative to the smectic layers are significant. A corrugated potential, in which the crosslink points sit is illustrated in Fig. 13. Deviation of crosslink points from these wells is penalized because the ensuing disruption of the smectic order of the layers, and because of the steric repulsion between crosslinks and the mesogens [17]. Here we ignore the additional penalty incurred by segments of the polymer chain by virtue of their crossing the smectic layers. This could be corrected for to some extent by putting in an effective value of the anisotropy, r. There is evidence [18] that homopolymer networks, where the smectogens are not diluted, experience a strong potential [as evidenced by their extreme Poisson ratios (0, 1)]. On the other hand, dilution takes one to the other limit, namely a smectic elastomer where the layer modulus is too low to influence the solid elasticity [18]. The interaction of crosslinks with a smectic potential has been studied by Olmsted and Terentjev [17]. These authors were interested in the limit of weak potentials since they described the character of the nematic to Sm-*A* transition in the presence of randomness induced in this manner. We explore instead the effect of strong potentials.

Taking account of the Gaussian distribution of interlink chain configurations and the additional weight given to the

end positions by the smectic potential, the probability distribution of the ends of the chain, $\mathbf{R}_1$ and $\mathbf{R}_2$ is

$$P_0(\mathbf{R}_1,\mathbf{R}_2) \propto \exp\Bigg(-\frac{3}{2L}\mathbf{R}_{12}^T\cdot\underline{\underline{l}}_0^{-1}\cdot\mathbf{R}_{12}+2\beta\cos(\alpha-\mathbf{q}_0^T\cdot\mathbf{R}_1) + 2\beta\cos(\alpha-\mathbf{q}_0^T\cdot\mathbf{R}_2)\Bigg), \tag{61}$$

$$\approx\sum_{n,m}\exp\Bigg(-\frac{3}{2L}\mathbf{R}_{12}^T\cdot\underline{\underline{l}}_0^{-1}\cdot\mathbf{R}_{12}-\beta(2\pi n-\mathbf{q}_0^T\cdot\mathbf{R}_1+\alpha)^2 - \beta(2\pi m-\mathbf{q}_0^T\cdot\mathbf{R}_2+\alpha)^2\Bigg), \tag{62}$$

$$=\sum_{m,n}P_{0(m,n)}(\mathbf{R}_1,\mathbf{R}_2), \tag{63}$$

where $\mathbf{R}_{12}=\mathbf{R}_1-\mathbf{R}_2$, L is the arc length of a polymer, $\mathbf{q}_0$ is the wave vector of the smectic layers, α is an additional phase if layers are displaced with respect to the matrix, and $\beta=V_s/k_BT$ defines the strength of the smectic layer potential in which the crosslinks sit, divided by k_BT. Unlike [3,7,17] we are only interested in the uniform (nonfluctuating) displacement fields for the matrix and layers. The step length definition is as in Eq. (7) but without a factor of $\ell_\perp$ yet taken out as in that dimensionless form

$$\underline{\underline{l}}_0=\ell_\perp\underline{\underline{\delta}}+(\ell_\parallel-\ell_\perp)\mathbf{n}_0\mathbf{n}_0^T. \tag{64}$$

We also assume, without loss of generality, that the first layer in the system sits at the origin $\alpha=0$, i.e., there is no displacement w.r.t. the background. In Eq. (62) we have taken the limit of $\beta\gg1$ and written the probability distribution as a sum over all the layers labelled by n and m in which the two different ends can sit. We have written the cosine functions as a power series and, since $\beta\gg1$, only the first term is significant. We can then bring down the summation sign from the exponent because β is so large all the wells of the potential are effectively decoupled. This expression is useful when quenching ends into a layer at crosslinking. The component (z) along the layer normal of this probability distribution is of the form $f(z)\propto e^{-z^2-\cos(z)}$. In the limit of strong potential, the peaks are separated and one can replace this function by a sum over Gaussian peak shapes displaced from the origin by multiples of the layer spacing and modulated by the nematic Gaussian $\exp[-(3/2L)z\ell_\parallel^{-1}z]$.

It is useful to convert to center of mass and relative coordinates in both spans and layers

$$\mathbf{P}=\frac{1}{2}(\mathbf{R}_1+\mathbf{R}_2),\quad \mathbf{Q}=(\mathbf{R}_1-\mathbf{R}_2), \tag{65}$$

$$p=(n+m),\quad r=(n-m). \tag{66}$$

The Jacobian from this change of variables for the following integrals cancel with the same factor in the normalization of the probabilities. The exponent in Eq. (62) then contains the following:

$$-\frac{3}{2L}\mathbf{Q}\cdot\underline{\underline{l}}_0^{-1}\cdot\mathbf{Q}-\frac{1}{2}\beta(2\pi r-\mathbf{q}_0^T\cdot\mathbf{Q})^2-2\beta(\pi p-\mathbf{q}_0^T\cdot\mathbf{P})^2. \tag{67}$$

When the smectic elastomer is formed deep in the smectic phase, the specific layer that the crosslink points are in will be a quenched variable, that is both p and r are quenched variables. When the crosslinks are formed the span of the polymer, $\mathbf{Q}$, is quenched in, and since both the ends of the chain are fixed into a network then so must the coordinate $\mathbf{P}$ also be quenched.

We now deform the matrix by $\underline{\underline{\lambda}}$ so that $\mathbf{P}\to\underline{\underline{\lambda}}\cdot\mathbf{P}$, then translate it by $\mathbf{u}$, and finally translate the smectic layers parallel to their *new* normal by v. Only the centre of mass part with $\mathbf{P}$ (and not the relative part with $\mathbf{Q}$) in the energy is changed. The last term in Eq. (67) on transforming the solid plus layers becomes

$$2\beta[2\pi v/d+\pi p-\mathbf{q}^T\cdot(\underline{\underline{\lambda}}\cdot\mathbf{P}+\mathbf{u})]^2.$$

Note that the phase picked up by layer translation involves the new spacing d rather than that before deformation d_0 in the first term and likewise in the last term it is the new wave vector $\mathbf{q}^T$ that enters. To calculate the free energy of the system we must complete the following quenched average of this energy over the probability of the formation conditions:

$$f=-k_BT\int d\mathbf{P}\int d\mathbf{Q}\sum_p\sum_r P_{0(p,r)}(\mathbf{P},\mathbf{Q})\ln\{P_{(p,r)}[(\underline{\underline{\lambda}}\cdot\mathbf{P}+\mathbf{u}),\underline{\underline{\lambda}}\cdot\mathbf{Q}]\}, \tag{68}$$

$$=\frac{k_BT}{\mathcal{N}}\iint d\mathbf{P}d\mathbf{Q}\sum_p\sum_r\exp\Bigg[-\frac{3}{2L}\mathbf{Q}\cdot\underline{\underline{l}}_0^{-1}\cdot\mathbf{Q}-\frac{1}{2}\beta(2\pi r-\mathbf{q}_0^T\cdot\mathbf{Q})^2-2\beta(\pi p-\mathbf{q}_0^T\cdot\mathbf{P})^2\Bigg]\Bigg(\frac{3}{2L}\mathbf{Q}^T\cdot\underline{\underline{\lambda}}^T\cdot\underline{\underline{l}}^{-1}\cdot\underline{\underline{\lambda}}\cdot\mathbf{Q} + \frac{\beta}{2}[2\pi r-\mathbf{q}^T\cdot\underline{\underline{\lambda}}\cdot\mathbf{Q}]^2+2\beta[2\pi v/d+\pi p - \mathbf{q}^T\cdot(\underline{\underline{\lambda}}\cdot\mathbf{P}+\mathbf{u})]^2\Bigg). \tag{69}$$

Here $\mathcal{N}$ is the normalization constant for the probability distribution. This integral can be separated out into an integral over $\mathbf{P}$ and an integral over $\mathbf{Q}$. The first gives the vital foundations of smectic rubber elasticity—the coupling between layer and matrix displacements and the rotation of layers with the deformation of the matrix. The second will give the actual form of the smectic rubber elastic energy. We tackle these two integrals one at a time.

The $\mathbf{P}$ integral is

$$\frac{1}{\mathcal{N}}\int d\mathbf{P}\sum_p\exp[-2\beta(\mathbf{q}_0^T\cdot\mathbf{P}-\pi p)^2] \times\{2\beta[2\pi v/d+\pi p-\mathbf{q}^T\cdot(\underline{\underline{\lambda}}\cdot\mathbf{P}+\mathbf{u})]^2\}.$$

To perform the sum over p we first note that $\beta\gg1$ so that we have a very narrow Gaussian distribution and the particular

value $p=(1/\pi)\mathbf{q}_0^T\cdot\mathbf{P}$ is picked out. The resulting expression is

$$\frac{1}{\mathcal{N}}\int d\mathbf{P}(2\beta[2\pi v/d-\mathbf{q}^T\cdot(\underline{\underline{\lambda}}\cdot\mathbf{P}+\mathbf{u})+\mathbf{q}_0^T\cdot\mathbf{P}]^2)$$
$$=2\beta\left((2\pi v/d-\mathbf{q}^T\cdot\mathbf{u})^2+\frac{\mathcal{L}_i^2}{12}(\mathbf{q}^T\cdot\underline{\underline{\lambda}}-\mathbf{q}_0^T)_i^2\right), \quad (70)$$

on doing the **P** integral as well. This expression, though an energy density, contains in the strain term the size of the system in the *i*th direction, $\mathcal{L}_i$, since the integral is not governed. The term is so large because if the layers were to rotate relative to the network in such a way as to not be commensurate with the crosslink points, then all of the crosslinks throughout the whole sample would be displaced from the minimum in the smectic potential by an amount scaling with the lineal dimension of the system, resulting in a massive energy cost. This otherwise large term can be made zero (minimized) only if $\mathbf{q}^T\cdot\underline{\underline{\lambda}}$ and $\mathbf{q}_0^T$ are parallel. Their magnitudes can be made to agree by modifying *d* which is penalized separately by the modulus *B*. *Thus the rotation of the layers with the applied deformation is a rigid constraint*:

$$\mathbf{q}=\underline{\underline{\lambda}}^{-T}\cdot\mathbf{q}_0. \quad (71)$$

This result is the microscopic justification of the geometric results (3) and (4). The total rigidity of the constraint on layers and shears was first obtained in [3].

The first term of Eq. (70) describes the penalty associated with a mismatch between the smectic layers and the matrix arising from translation of one relative to the other. Multiplying by the number of network strands per unit volume, n_s, gives the associated free energy density

$$f_{\rm rel}=2k_BT\beta\left(\frac{2\pi}{d}\right)^2 n_s(v-\mathbf{n}\cdot\mathbf{u})^2\equiv\frac{1}{2}\Lambda(v-\mathbf{n}\cdot\mathbf{u})^2$$

with

$$\Lambda=16\pi^2\mu V_s/(k_BTd^2). \quad (72)$$

This layer-matrix coupling has been used in continuum models [3,6] and in [7] where it was estimated phenomenologically, see also [10]. Connection can also be made roughly to the polymer scale via $R_0^2\sim Nd^2$ where $R_0^2\sim\ell L$ has previously been introduced as a characteristic mean square dimension, here for a chain with *N* links. Also the smectic scale enters as $V_s\sim k_BT|\psi|^2$. Then our estimate of Λ is

$$\Lambda=16\pi^2\mu N|\psi|^2/R_0^2.$$

The cost of uniform relative translation decouples from the cost of shears and shear-layer rotation/dilation, and we do not employ it in our nonlinear elastic analysis.

To obtain the rubber elastic part of the free energy, we now consider the integral over the variable **Q** (suppressing the normalization $1/\mathcal{N}$):

$$\int d\mathbf{Q}\sum_r\exp\left(-\frac{3}{2L}\mathbf{Q}\cdot\underline{\underline{l}}_0^{-1}\cdot\mathbf{Q}-\frac{1}{2}\beta(2\pi r-\mathbf{q}_0^T\cdot\mathbf{Q})^2\right)$$
$$\times\left(\frac{3}{2L}\mathbf{Q}^T\cdot\underline{\underline{\lambda}}^T\cdot\underline{\underline{l}}^{-1}\cdot\underline{\underline{\lambda}}\cdot\mathbf{Q}+\frac{\beta}{2}(2\pi r-\mathbf{q}^T\cdot\underline{\underline{\lambda}}\cdot\mathbf{Q})^2\right). \quad (73)$$

We use the same procedure as that carried out for the previous integral; first the sum over *r* is evaluated picking out the particular value $r=(1/2\pi)\mathbf{q}_0^T\cdot\mathbf{Q}$, and then the integral over **Q** performed. After carrying out the sum over *r* we obtain

$$\int d\mathbf{Q}\,\exp\left(-\frac{3}{2L}\mathbf{Q}\cdot\underline{\underline{l}}_0^{-1}\cdot\mathbf{Q}\right)\cdot\left(\frac{3}{2L}\mathbf{Q}^T\cdot\underline{\underline{\lambda}}^T\cdot\underline{\underline{l}}^{-1}\cdot\underline{\underline{\lambda}}\cdot\mathbf{Q}\right.$$
$$\left.+\frac{\beta}{2}(\mathbf{q}_0^T\cdot\mathbf{Q}-\mathbf{q}^T\cdot\underline{\underline{\lambda}}\cdot\mathbf{Q})^2\right).$$

The integral over **Q** can then be performed. The first term results in the usual trace formula expression. The second term can be evaluated using the average: $\langle\mathbf{Q}^T\mathbf{Q}\rangle=\frac{1}{3}L\underline{\underline{l}}_0$. The result is then

$$\frac{L\beta}{6}\mathrm{Tr}[\underline{\underline{l}}_0\cdot(\mathbf{q}_0\cdot\mathbf{q}_0^T-\underline{\underline{\lambda}}^T\cdot\mathbf{q}\cdot\mathbf{q}^T\cdot\underline{\underline{\lambda}}-\underline{\underline{\lambda}}^T\cdot\mathbf{q}\cdot\mathbf{q}_0^T-\mathbf{q}_0\cdot\mathbf{q}^T\cdot\underline{\underline{\lambda}})]. \quad (74)$$

This expression can be simplified by using the definition of $\underline{\underline{l}}_0$ given in its dimensionful form Eq. (64). Since $\mathbf{n}_0$ and $\mathbf{q}_0$ are parallel we have

$$\frac{L\beta}{6}\mathrm{Tr}\left[\left(\frac{2\pi}{d_0}\right)^2\ell_\parallel\underline{\underline{\delta}}-\underline{\underline{l}}_0\cdot\underline{\underline{\lambda}}^T\cdot\mathbf{q}\cdot\mathbf{q}^T\cdot\underline{\underline{\lambda}}-\underline{\underline{\lambda}}^T\cdot\mathbf{q}\cdot\mathbf{n}_0^T\frac{2\pi}{d_0}\ell_\parallel\right.$$
$$\left.-\frac{2\pi}{d_0}\ell_\parallel\mathbf{n}_0\cdot\mathbf{q}^T\cdot\underline{\underline{\lambda}}\right]. \quad (75)$$

This expression can be rearranged into

$$\frac{L\beta}{6}\left((\underline{\underline{l}}_0^{1/2}\cdot\underline{\underline{\lambda}}^T\cdot\mathbf{q})-\frac{2\pi}{d_0}\mathbf{n}_0\sqrt{\ell_\parallel}\right)^2. \quad (76)$$

It can be seen from this expression that this constraint also penalizes **q** if it is not equal to $\underline{\underline{\lambda}}^{-T}\cdot\mathbf{q}_0$. The resulting terms from the **Q** integral are thus.

$$\frac{1}{2}\mathrm{Tr}(\underline{\underline{\lambda}}\cdot\underline{\underline{l}}_0\cdot\underline{\underline{\lambda}}^T\cdot\underline{\underline{l}}^{-1})+\frac{1}{2}\frac{L\beta}{3}\left[(\underline{\underline{l}}_0^{1/2}\cdot\underline{\underline{\lambda}}^T\cdot\mathbf{q})-\frac{2\pi}{d_0}\mathbf{n}_0\sqrt{\ell_\parallel}\right]^2.$$

One converts these energies per strand into energy densities by multiplying by the strand number density n_s. Our final microscopic model for smectic liquid crystal elastomers is:

$$f=\frac{1}{2}\mu\,\mathrm{Tr}(\underline{\underline{\lambda}}\cdot\underline{\underline{l}}_0\cdot\underline{\underline{\lambda}}^T\cdot\underline{\underline{l}}^{-l})+\frac{1}{2}B\left(\frac{d}{d_0}-1\right)^2, \quad (77)$$

where $\mu=k_BTn_s$. The second term is the layer compression penalty from the smectic free energy. We also make the identification of the layer normal, **q** with the director, **n**, and rigidly impose the constraint: $\mathbf{q}=\underline{\underline{\lambda}}^{-T}\cdot\mathbf{q}_0$. This returns us to our starting point, Eq. (10), but from a statistical mechanics point of view of the system.

VI. CONCLUSIONS

In conclusion, we have derived a model of Sm-*A* elastomers from both a geometric view point and from a microscopic model of the effect of a corrugated potential on the crosslink points in the smectic elastomer. This model reproduces the experimentally observed elastic behavior when the elastomer is stretched parallel or perpendicular to the layer normal. Most notable is the correlation between threshold strains and ratios of the various moduli that are found, along with the description of a characteristic, singular layer rotation with applied strain. The response to the two basic shears is also predicted but has not yet been observed. Our model also provides an explanation of the observed x-ray scattering patterns when the appropriate microstructure is considered.

ACKNOWLEDGMENTS

We thank E. M. Terentjev for critical remarks on our manuscript, in particular for penetrating comments about Sec. V, R. B. Meyer for discussions on de Vries phases, and S. M. Clarke for advice on x-ray scattering. M.W. is grateful for discussions about layer localization with T. C. Lubensky and L. Radzihovsky.

[1] E. Nishikawa and H. Finkelmann, Macromol. Chem. Phys. **200**, 312 (1999).
[2] N. A. Clark and R. B. Meyer, Appl. Phys. Lett. **22**, 493 (1973).
[3] T. C. Lubensky, E. M. Terentjev, and M. Warner, J. Phys. II **4**, 1457 (1994).
[4] E. Nishikawa, H. Finkelmann, and H. R. Brand, Macromol. Rapid Commun. **18**, 65 (1997).
[5] E. M. Terentjev and M. Warner, J. Phys. II **4**, 111 (1994).
[6] J. Weilepp and H. R. Brand, Macromol. Theory Simul. **7**, 91 (1998).
[7] M. J. Osborne and E. M. Terentjev, Phys. Rev. E **62**, 5101 (2000).
[8] O. Stenull and T. C. Lubensky, Phys. Rev. Lett. **94**, 018304 (2004).
[9] L. Golubovic and T. C. Lubensky, Phys. Rev. Lett. **63**, 1082 (1989).
[10] M. Warner and E. M. Terentjev, *Liquid Crystal Elastomers* (Oxford University Press, Oxford, 2003).
[11] P. G. de Gennes, in *Polymer Liquid Crystals*, edited by A. Ciferri, W. R. Krigbaum, and R. B. Meyer (Academic, New York, 1982).
[12] H. Finkelmann, I. Kundler, E. M. Terentjev, and M. Warner, J. Phys. II **7**, 1059 (1997).
[13] R. Stannarius, R. Köhler, U. Dietrich, M. Lösche, C. Tolksdorf, and R. Zentel, Phys. Rev. E **65**, 041707 (2002).
[14] S. Conti, A. de Simone, and G. Doltzmann, J. Mech. Phys. Solids **50**, 1431 (2002).
[15] D. J. Read, R. A. Duckett, J. Sweeney, and T. C. B. McLeish, J. Phys. D **32**, 2087 (1999).
[16] L. Radzihovsky and J. Toner (private communication).
[17] P. D. Olmsted and E. M. Terentjev, Phys. Rev. E **53**, 2444 (1996).
[18] R. Stannarius, R. Köhler, M. Rössler, and R. Zentel, Liq. Cryst. **31**, 895 (2004).